International Forum on Aeroelasticity and Structural Dynamics
IFASD 2017
25-28 June 2017, Como - Italy

NUMERICAL SIMULATION OF TRANSONIC FLUTTER OF A T-TAIL

K. ISOGAI

Professor Emeritus, Kyushu University, Fukuoka, Fukuoka 819-0395, Japan
koji.isogai@nifty.com

Keywords: transonic, flutter, T-tail, CFD, Navier-Stokes code.

Abstract: The numerical simulations of transonic flutter of a T-tail are conducted using a 3D Navier-Stokes code which takes into account the in-plane motion of the horizontal tail plane (HTP). As the result of the simulation, the sharp transonic dip phenomenon of the flutter boundary, which is similar to that experienced in the transonic flutter experiment conducted at NASA for the T-tail of a wide-body transport airplane in 1975, is predicted. In the present simulation, the effect of angle of attack of the HTP on the flutter boundary and the characteristics of the flutter are also examined in detail. Most of the flutter and limit cycle oscillation (LCO) experienced around the bottom of the dip are the single-degree-of-freedom flutter where the first bending mode of the vertical tail plane is predominant.

1 INTRODUCTION

The T-tail flutter speed depends strongly on the angle of attack or dihedral angle of the horizontal tail plane (HTP). (Note that the flutter speed of a conventional (single) wing does not depend on the angle of attack in the case of subsonic flight unless flow separation occurs.) This phenomenon was first recognized through the investigation of an accident involving a Handley Page Victor which was lost due to T-tail flutter in 1954 [1]. The mechanism of the phenomenon can be explained by the fact that the rolling moment generated by the yawing and sideslip oscillation of the HTP, which is induced by the torsion and bending oscillations of the vertical tail plane (VTP), depends on the angle of attack (or steady lift) and the dihedral angle of the HTP. Ruhlin et al. [2] conducted experimental studies of transonic T-tail flutter for a wide-body transport airplane. They found that the transonic flutter boundary of the anti-symmetric flutter of this T-tail showed an unusually sharp dip between the Mach numbers 0.92 and 0.98. This phenomenon clearly shows the importance of establishing the prediction method of

T-tail flutter, especially, in the transonic regime. Recently, computational fluid dynamics (CFD) has been applied to the transonic flutter of T-tail configurations [3,4]. Arizono et al. [3] presented the numerical simulations of a T-tail configuration using an Euler code. They also compared their results with experimental data, although the results of their numerical simulation show a considerable discrepancy with those of the experiment. Additionally, in their studies, the effects of the angle of attack and the dihedral angle of the HTP were not studied in detail. Attorni et al. [4] also conducted the T-tail flutter simulation of P180 aircraft using an Euler code. However, the accuracy of the method was not confirmed because no comparison with the experimental data was made. Isogai [5] presented a numerical method for computing the subsonic and transonic flows for a wing oscillating in yaw and sideslip using 3D Navier-Stokes (NS) equations as the first step towards a complete T-tail configuration. He showed that, by introducing a new coordinate system oscillating in yaw and sideslip, the existing 3D NS code can easily be modified to account for in-plane motions. The calculated rolling moments showed good agreement with the existing experimental data obtained for incompressible flow, and the effect of compressibility, especially the effects of the shock wave in the transonic flow on the rolling moment, is clarified. Isogai [6] extend the method proposed for a single wing to a T-tail configuration, for which the effect of in-plane motion of the HTP is taken into account, and clarified the effects of the in-plane motion of the HTP on the rolling moment around the HTP especially in transonic region. The purpose of the present paper is to apply the NS code thus developed for a T-tail configuration to the transonic flutter simulation of the T-tail of a transport airplane.

2 NUMERICAL METHOD (3D NAVIER-STOKES CODE)

As to the numerical method to take into account the effect of the in-plane motion of the HTP, we utilize the same method proposed by Isogai [6]; that is, we introduce new coordinate system that moves with the in-plane motion of the HTP. Figure 1 shows the definitions of the coordinate systems. The xyz coordinate system is fixed to the free-stream and the *x'y'z'* coordinate system is the coordinate system that moves with the in-plane motion of the HTP. (In Fig. 1, h_s and h_f are the displacements of the HTP and VTP normal to their time mean surfaces, respectively.) The relation between the two coordinate systems can be given by

$$x = x' + \Psi z' \quad y = y' \quad z = z' + H - \Psi(x' + a) \qquad (1)$$

where H and Ψ are the sideslip and yawing displacements of the HTP, respectively, and where the higher-order terms of Ψ are neglected. (Note that length is made non-dimensional by the semichord (b) at the junction.) The conventional 3D NS code can be easily modified by changing the metric terms such as ξ_x, ξ_y, ξ_z, etc., which

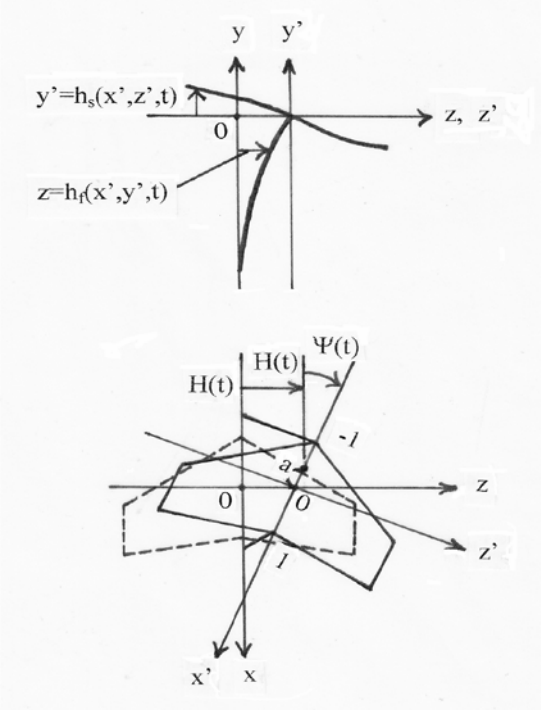

Figure 1: Definitions of coordinate systems.

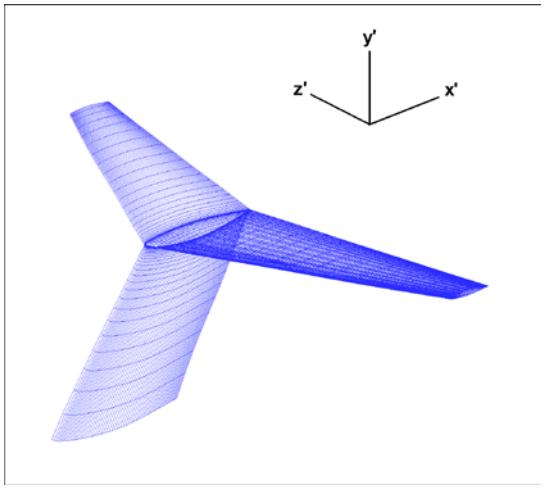

Figure 2: Surface grid of model T-tail.

transform the 3D NS equations in the *xyz* coordinate system into the computational space (ξ, η, ζ) [6].

The T-tail used for the present study is that of one of the prototypes of the research airplane (ASUKA) [7] developed by JAXA for the study of short-take-off landing (STOL) technology. In Fig. 2, the plan forms of the HTP and VTP are shown together with the surface grid distributions for the present CFD computations. The span, chord length at the junction, taper ratio and sweptback angle of the 25% chord line of HTP are 14.8 m, 3.81 m, 0.315 and 25 deg, respectively, and those of VTP are 4.87 m, 3.81 m, 0.860 and 30 deg, respectively. The airfoil sections of HTP and VTP are NACA65A010. The Reynolds Averaged Navier-Stokes (RANS) code originally developed by Isogai [6] is used for the present numerical simulation. The grid is a H-H type structured grid. The number of grid point around the HTP is 120 points in the x' direction (61 points on the upper/lower surfaces, respectively), 66 points in the y' direction (31/35 points normal to the upper/lower surfaces, respectively) and 78 points in the z' direction (58 points on the wing surface). The number of grid point around the VTP is 120 points in the x' direction

(61 points on the upper/lower surfaces, respectively), 35 points in the y' direction and 78 points in the z' direction (39 points normal to the upper/lower surfaces, respectively). The code utilizes the Total Variation Diminishing (TVD) scheme [8]. Reynolds number is assumed to be 10^6 and Baldwin & Lomax turbulence model [9] is employed. The accuracy and the reliability of the present code were well examined in Ref. 6.

3 NATURAL VIBRATION ANAYSIS

The beam model and the lumped parameter method [10] are used to find the natural vibration modes and frequencies. The schematic figure and dimension of the present beam model are shown in Fig. 3. Since we are interested in the anti-symmetric T-tail flutter, the HTP is assumed to be rigid. Since the maximum Mach number of ASUKA is 0.565, the original stiffness of the body and T-tail of ASUKA is increased for the present T-tail model so that flutter might occur in the transonic regime, namely, the *EI* and *GJ* of the half body and the VTP of the present T-tail model are set to be $EI=7.0(EI)_o$ and $GJ=4.2(GJ)_o$, where $(EI)_o$ and $(GJ)_o$ are those of the original ASUKA. The location and the swept back angle of the elastic axis are 38.7 percent chord from the leading edge of VTP and 29 deg, respectively. In table 1 (see the appendix), the mass properties along the elastic axis of the half body and the VTP, and those of the HTP are shown. In the table, m(s), $S_y(s)$, $I_y(s)$ are the distributions of mass, static unbalance and moment of inertia along the elastic axis, and I_α is the moment of inertia at the junction of the half body and the VTP, and M_{HTP}, S_{HTP}, I_Ψ and I_ϕ are the mass, static unbalance, moment of inertias around the yaw and roll axis of the HTP, respectively. In table 2 (see the appendix), EI and GJ along the elastic axis of the half body and the VTP are shown. The first 3 natural frequencies and mode shapes are shown in Fig. 4 (the other natural frequencies are f_4=25.35 Hz, f_5=45.13 Hz and f_6=51.16 Hz). The six natural mode shapes and the frequencies are used for the

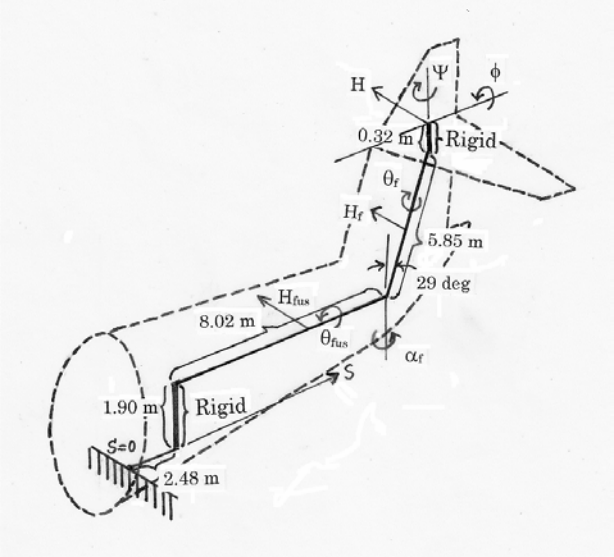

Figure 3: Beam model for natural vibration analysis.

aeroelastic response computations, which are discussed in the next section.

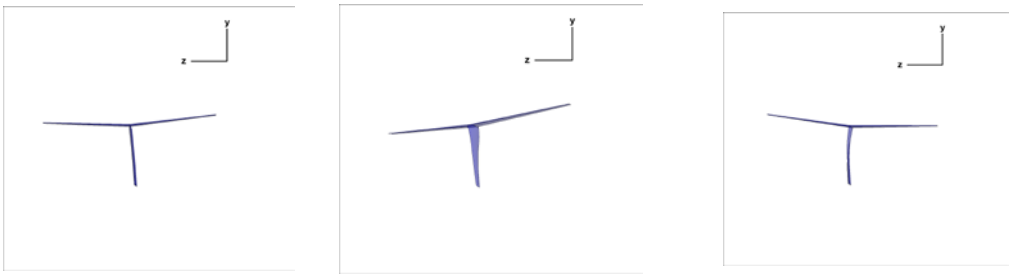

1st bending, f_1=3.09 Hz 1st torsion, f_2=5.02 Hz 2nd bending, f_3=14.14 Hz

Figure 4: Natural vibration mode of model T-tail.

4 AEROELASTIC RESPONSE COMPUTATIONS

We use the modal approach for the aeroelastic response computations. The displacements of HTP and VTP normal to the surfaces are expressed using the six natural mode shapes of them as follows:

$$H_{HTP}(X',Z',t)=\sum_{i=1}^{6}\phi_i Z' q_i \tag{2}$$

$$H_{VTP}(X',Y',t)=\sum_{i=1}^{6}H_{VTP,i}(X',Y')q_i \tag{3}$$

$$H(t)=\sum_{i=1}^{6}H_i q_i \quad (4), \qquad \Psi(t)=\sum_{i=1}^{6}\Psi_i q_i \tag{5}$$

where H_{HTP} and H_{VTP} are the displacements normal to the surfaces of HTP and VTP, respectively, and where ϕ_i and $H_{VTP,i}$ are the i-th natural mode shapes of the roll angle of HTP and the displacement normal to the surface of the VTP, respectively. H(t) and Ψ(t) are the sideslip and yaw angle of the HTP, and H_i and Ψ_i are the i-th natural mode shapes of the sideslip and yaw angle of the HTP, respectively. Eqs. (2) ~ (5) are used to generate the grid around the T-tail.

The aeroelastic response is computed by solving the following ordinary differential equations for the unknown generalized coordinate q_i:

$$M_i d^2 q_i/dt^2+\omega_i g_i M_i dq_i/dt+\omega_i^2 M_i q_i=Q_i \qquad \text{i=1,…., 6} \tag{6}$$

where M_i is the generalized mass, and it is given by

$$M_i=\int_{FUS}\left\{m(s)H_{fus,i}^2(s)-2S_y(s)H_{fus,i}(s)\theta_{fus,i}(s)+I_y(s)\theta_{fus,i}^2(s)\right\}ds$$

$$+\int_{VTP}\left\{m(s)H_{f,i}^{2}(s)-2S_{y}(s)H_{f,i}(s)\theta_{f.i}(s)+I_{y}(s)\theta_{f,i}^{2}(s)\right\}ds$$

$$+I_{\alpha}\alpha_{f,i}^{2}+M_{HTP}H_{i}^{2}-2S_{HTP}H_{i}\Psi_{i}+I_{\Psi}\Psi_{i}^{2}+I_{\phi}\phi_{i}^{2}\quad \text{i=1, ….., 6} \qquad (7)$$

where the $H_{fus,i}$, $\theta_{fus,i}$, ……., etc. are the i-th natural mode shapes of the bending and torsion displacements along the elastic axis of the half body and the VTP, and the side-slip, yawing and rolling displacements of the HTP, respectively (the definitions of them are shown in Fig. 3).

In Eq. (6), ω_i is the i-th natural circular frequency, g_i is the damping coefficient and Q_i is the generalized aerodynamic force, and it is given by

$$Q_{i}=\iint_{VTP}\Delta P(X',Y')H_{VTP,i}(X',Y')dS+R_{M}\phi_{i} \qquad \text{i=1,…...., 6} \qquad (8)$$

where ΔP is the pressure difference on the VTP and where R_M is the rolling moment around the HTP. ΔP and R_M are computed using the 3D Navier-Stokes code described in Section 2. Equation (6) and the 3D Navier-Stokes equations are solved at each time step to obtain the aeroelastic response of the model T-tail.

5 RESULTS OF AEROELASTIC RESPONSE COMPUTATIONS

Before we present the results of the aeroelastic response computations it might be worthwhile to point out the characteristics of transonic T-tail flutter. Namely, there is a large mass of HTP at the top of the VTP (the mass of the HTP of ASUKA is about 65% of the total mass of the T-tail). Therefore, the mass ratio of T-tail is very large compared with a conventional wing configuration. This means that the flutter of T-tail might experience the large transonic dip since the mechanism of a single-degree of freedom flutter of the first bending mode of VTP might be predominant as pointed out in Reference 11.

The aeroelastic response computations are conducted for the angle of attack of HTP, namely, α_H=0 deg and α_H=5 deg at the altitude of 10,000 m, respectively. The dihedral angle of HTP is assumed to be zero for both cases. The sound velocity at 10,000 m is 299.532 m/s.

5.1 Results of α_H=0 deg

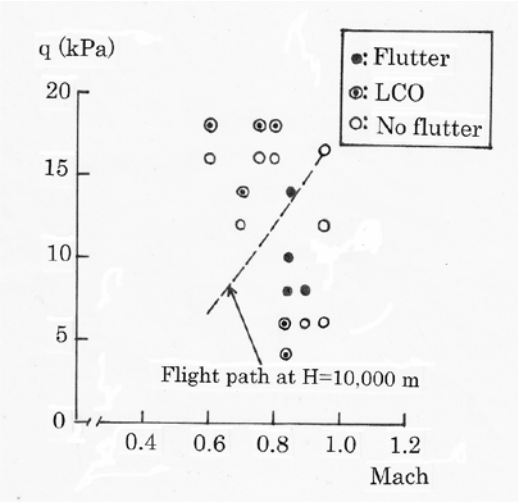

Figure 5: Results of aeroelastic response computations for α_H=0 deg.

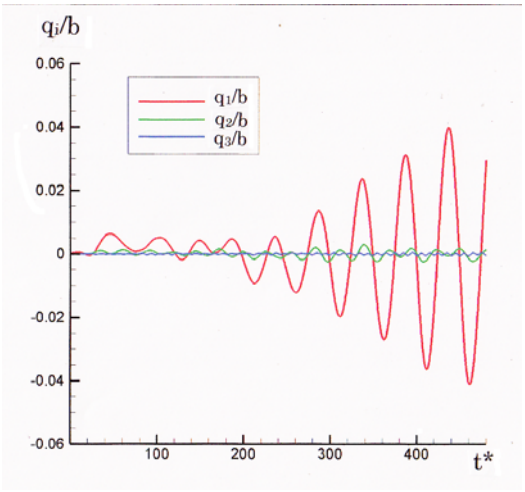

Figure 6: Time history of generalized coordinates at M_∞=0.90 and q=8.0 kPa.

The aeroelastic response computations were conducted for 18 cases of the different combinations of Mach numbers from 0.60 to 0.95 and of dynamic pressures from 4.0 kPa to 18 kPa. The results are plotted in Fig. 5 and the numerical data of them are given in Table 3 (see the appendix). The dotted line in the figure indicates the flight path at the altitude of 10,000 m. In Table 1, the frequency of flutter and limit cycle oscillation (LCO), the mass ratio μ_F and the amplitude ($|H|$) of LCO are also shown. The mass ratio μ_F is defined by

$$\mu_F = \frac{M_t}{\pi\rho b^2 l_f (\lambda_f + (1-\lambda_f)^2/3.0)} \tag{9}$$

where M_t is the total mass of the T-tail (1,919 kg) which is the sum of the masses of the HTP (1,241 kg) and the VTP (678 kg), b is the semichord length at the junction of HTP and VTP, l_f is the span (4.865 m) of VTP, and λ_f is the taper ratio of VTP, respectively. The amplitude of LCO ($|H|$) is defined by the maximum amplitude of the sideslip oscillation of the HTP. (It should be noted that the cases whose amplitude of LCO is less than 10 mm are tentatively indicated as “No flutter” in both Figures 5 and 10, and Tables 3 and 4, respectively.)

As seen in Fig. 5, a sharp transonic dip is observed between Mach numbers 0.85 and 0.90, which is similar to that observed in the transonic flutter experiment conducted by Ruhlin et al. [2] for the T-tail of the wide body transport airplane in 1975. Figure 6

shows the time histories of the first three generalized coordinates (q_i/b, i=1-3) obtained at the bottom of the dip (Case 15, M_∞=0.90, dynamic pressure q=8.0 kPa, t*is the non-dimensional time defined by t*=tV/b.). The figure clearly shows that the first mode is predominant and it is a single-degree of freedom flutter. It can be confirmed also from Table 3 that the flutter frequency is 2.84 Hz which is very close to the first natural frequency of 3.09 Hz. Figures 7 and 8 show the typical flow patterns (iso-density contour) around the HTP and VTP, respectively. As seen in the figures, the strong shock waves are observed at 75~80 percent chord from the leading edge of the HTP and at 60 ~ 75 percent chord from the leading edge of the VTP, respectively. Further decrease of dynamic pressure from 8.0 kPa at M_∞=0.90 to 6.0 kPa does not generate flutter, while at M_∞=0.85, the LCO of the second mode (the first torsion mode) predominant occurs at q=6.0 kPa (Case 10) and q=4.0 kPa (Case 9). In Fig. 9, the responses of the first three generalized coordinates at M_∞=0.85 and q=6.0 kPa are shown. The frequency of the LCO is 4.97 Hz which is very close to the second natural frequency of 5.02 Hz. At M_∞=0.95, no flutter nor LCO is obtained at the dynamic pressure up to q=16.7 kPa.

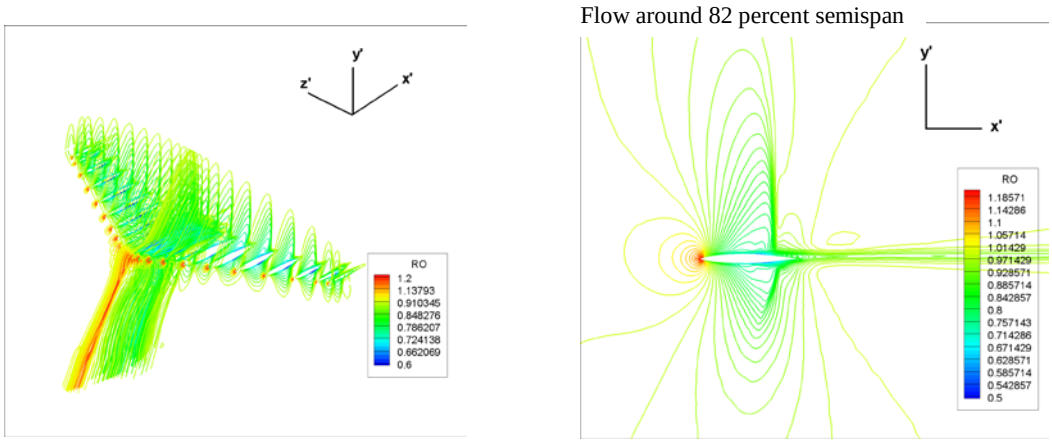

Figure 7: Flow pattern (iso-density contour) around HTP at M_∞=0.90, α_H=0 deg and q=8.0 kPa (density is made non-dimensional by free-stream density).

5.2 Results of α_H=5 deg

As explained in the introduction, the angle of attack of the HTP might give considerable effect on the flutter speed of T-tail. Results of the aeroelastic response computations obtained for α_H=5 deg are plotted in Fig. 10 and its numerical data are given in Table 4 (see the appendix). As seen in the figure, the sharp transonic dip is also observed between M_∞=0.85 ~ 0.95.

18 percent span from junction of VTP and HTP

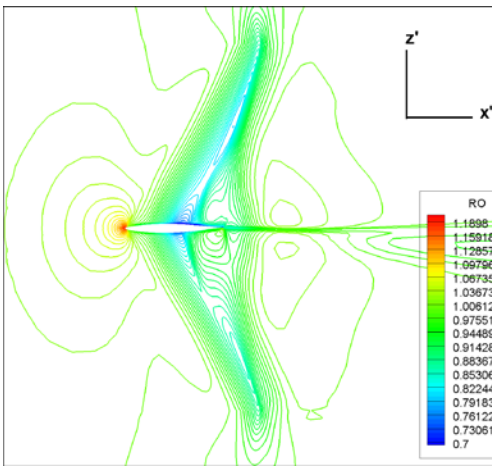

Figure 8: Iso-density contour around VTP
M_∞=0.90, α_H=0 deg and q=8.0 kPa.

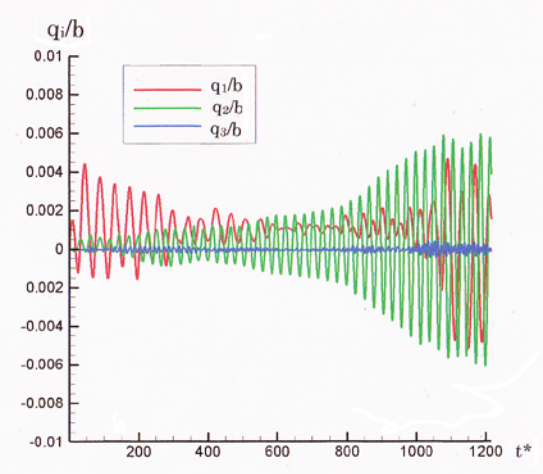

Figue 9: Time history of generalized coordinates
At M_∞=0.85, α_H=0 deg and q=6.0 kPa.

However the characteristics of the responses are considerably different from those obtained for α_H=0 deg. The hard flutter is observed at M_∞=0.75 and q=16.0 kPa and 18.0 kPa (Case 4 and Case 5 of Table 4), respectively. All the responses obtained between M_∞=0.85 and 0.90 (Case 7 ~ Case 16) where the sharp transonic dip is observed are LCO. However, the slowly diverging flutter is obtained at M_∞=0.95 and q=4.0 kPa (Case 17) and q=6.0 kPa (Case 18). Figure 11 shows the responses of the first 3 generalized coordinates (q_i/b, i=1-3) obtained at M_∞=0.95 and q=4.0 kPa (Case 17). As seen from the figure, it is a single-degree-of-freedom flutter of the first bending mode of the VTP whose frequency is 3.12 Hz which is close to the first natural frequency of 3.09 Hz. Figures 12 and 13 show the typical flow patterns (iso-density contour) around the VTP and the HTP, respectively. As seen in Fig. 12, the shock wave is observed at about 83 percent chord from the leading edge of the VTP, while, as seen in Fig. 13, the shock induced flow separation and the strong shock wave just after the trailing edge around

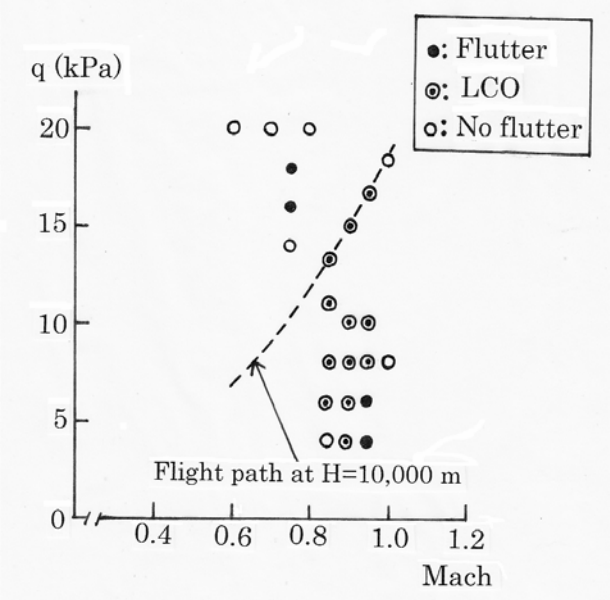

Figure 10: Results of aeroelastic response computations
for α_H=5 deg.

the HTP are observed. At M_∞=1.0, no flutter nor LCO is observed at dynamic pressure up to 18.65 kPa (case 22 and 23).

6 CONCLUDING REMARKS

The numerical simulations of the transonic flutter of a T-tail were conducted using a 3D Navier-Stokes code which takes into account the in-plane motion of the HTP. As the result of computation, a sharp transonic dip of the flutter boundary, which is similar to that experienced in the transonic flutter experiment conducted at NASA by Ruhlin et al. [2] for the T-tail of the wide body transport airplane in 1975, is predicted. The effect of the angle of attack (α_H) of the HTP was also examined in the present simulation. The transonic dip for α_H=0 deg was experienced between the Mach numbers 0.85 ~ 0.90, while it was experienced between the Mach numbers 0.85 ~ 0.95 for α_H=5 deg. The characteristics of flutter experienced around the dip are also very different between α_H=0 deg and α_H=5 deg, namely, they were mostly hard flutter for α_H=0 deg while they were mostly LCO for α_H=5 deg. Most of the flutter and LCO experienced around the bottom of the dip are a single-degree-of-freedom flutter where the fist bending mode of the VTP is predominant.

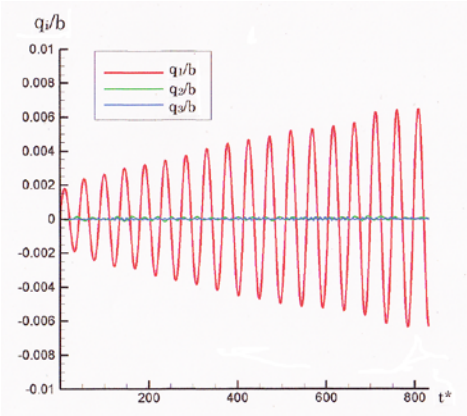

Figure 11: Time history of generalized coordinates at M_∞=0.95, α_H=5 deg and q=4.0 kPa.

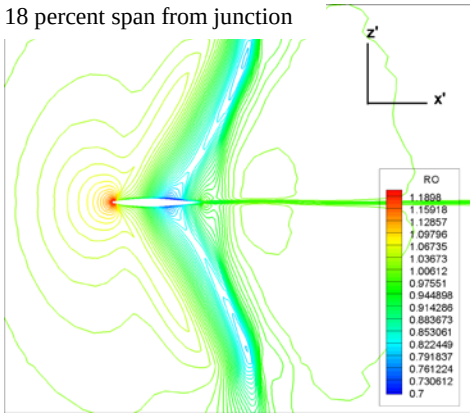

Figure. 12: Flow pattern (iso-density contour) around VTP at M_∞=0.95, α_H=5 deg and q=4.0 kPa.

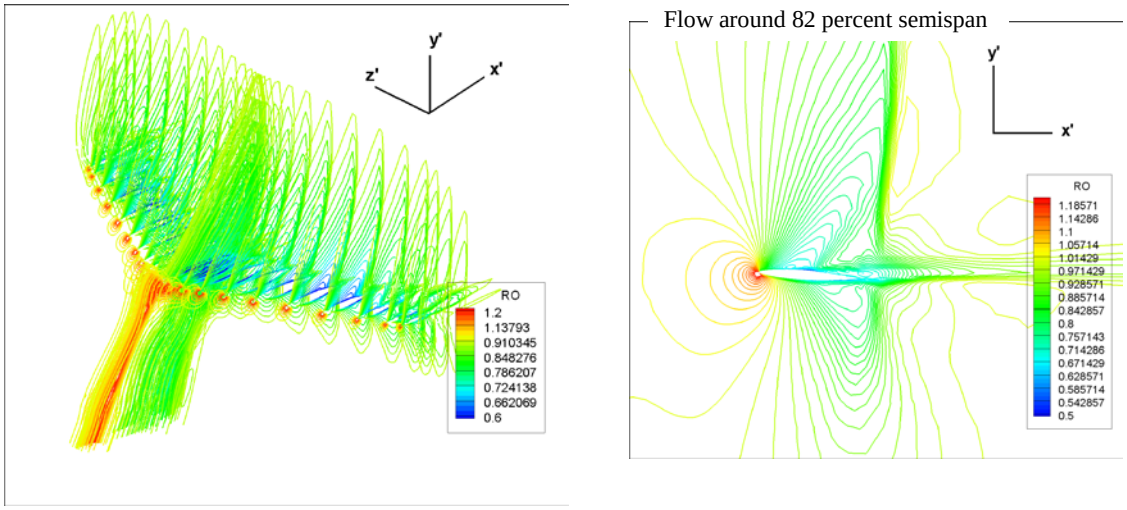

Figure 13: Flow pattern (iso-density contour) around HTP at

M_∞=0.95, α_H=5 deg and q=4.0 kPa.

6 REFERENCES

[1] Baldock, J. C. A. (1975). The determination of the flutter speed of a T-tail unit by calculations, model tests and flight flutter tests. Report 221, AGARD.

[2] Ruhlin. C. L. and Sandford, M. C. (1975). Experimental parametric studies of transonic T-tail flutter. TN D-8066, NASA.

[3] Arizono, H., Kheirandish, H. R. and Nakamichi, J. (2007). Flutter simulation of a T-tail configuration using non-linear aerodynamics. *International Journal for Numerical Methods in Engineering*, **72**, 1513-1523.

[4] Attorni, A., Cavagna, L. and Quaranta, G. (2011). Aircraft T-tail flutter predictions using computational fluid dynamics. *Journal of Fluids and Structures*, 27 161-174.

[5] Isogai, K. (2016). Subsonic and transonic flow simulation for a wing oscillating in yaw and sideslip. *Trans. Japan Soc. Aero. Space Sci.*, Vol. 59 (1), 18-24.

[6] Isogai, K. (2016). Subsonic and transonic flow simulation for an oscillating T-tail. *Trans. Japan Soc. Aero. Space Sci.*, Vol. 59 (1), pp. 25-32.

[7] STOL Aircraft Project Group (1981). Basic design of quiet short take-off and landing research aircraft. TM-452, NAL (in Japanese).

[8] Yee, H. C. and Harten, A. (1987). Implicit TVD scheme for hyperbolic conservation laws in curvilinear coordinate. *AIAA Jornal*, Vol. 25 (2), 266-274.

[9] Baldwin, B. C. and Lomax, H. (1978). Thin layer approximation and algebraic model for separated turbulent flows. Paper 78-257, AIAA.

[10] Bispringhoff, R. L., Ashley, H. and Halfman, R. L.(1955). *Aeroelasticity*. Cambridge, MA : Addison Wesley.

[11] Isogai, K. (1981). Transonic dip mechanism of flutter of a sweptback wing: Part II. *AIAA Journal*, Vol. 19 (9), 1240-1242.

COPYRIGHT STATEMENT

all of the original material included in paper. The authors also confirm that they have obtained permission, from the copy holder of any third party material included in this paper, to publish it as part of their paper. The authors confirm that they give permission, or have obtained permission from the copyright holder of this paper, for the publication and distribution of this paper as part of the IFASD-2017 proceedings or as individual off-prints from the proceedings.

Appendix

No.	s (m)	m (kg)	I_y (kgm^2)	S_y (kgm)
1	0.0	6.226×10^2	2.720×10^3	5.420×10^2
2	1.28	6.226	2.720	5.420
3	2.48	6.725	2.585	3.230
4	4.26	4.416	3.630	9.850
5	5.69	4.896	2.458	7.150
6	7.50	2.082	0.677	2.082
7	9.20	2.629	0.434	1.150
8	10.50	2.204	0.264	4.277
9	11.3	0.830	0.0408	-0.477
10	12.0	0.661	0.0350	-0.0073
11	12.3	0.406	0.101	0.642
12	12.7	0.994	0.0368	0.163
13	13.5	0.760	0.0540	-0.250
14	13.95	0.776	0.329	1.599
15	14.40	0.656	0.0295	-0.052
16	15.05	0.954	0.0339	-0.324
17	15.70	1.832	0.283	1.319
18	16.30	0.811	0.0612	0.791
19	16.35	0.0	0.0	0.0

$I_\alpha=2.390\times10^2$ km^2, $M_{HTP}=1.242\times10^3$ kg, $S_{HTP}=1.788\times10^3$ kgm, $I_\Psi=1.4977\times10^4$ kgm^2, $I_\phi=1.087\times10^4$ kgm^2

No. 1 – 8 : Half body, No. 9 – 19 : VTP

Table 1: Mass properties of model T-tail.

No.	s (m)	EI (Nm^2)	GJ (Nm^2)
1	0.0	1.029×10^{10}	4.651×10^{9}
2	1.28	1.029	4.651
3	2.48	0.926	4.651
4	4.26	0.535	0.790
5	5.69	0.514	0.535
6	7.59	0.473	0.358
7	9.20	0.415	0.235
8	10.50	0.340	0.169
9	11.30	0.0240	0.144
10	12.00	0.0268	0.159
11	12.30	0.0268	0.156
12	12.70	0.0259	0.149
13	13.50	0.0217	0.114
14	13.95	0.0202	0.110
15	14.40	0.0193	0.102
16	15.05	0.0187	0.100
17	15.70	0.0172	0.0387
18	16.30	0.0144	0.0387
19	16.35	0.0125	0.0387

No. 1 – 8 : Half body, No.9 – 19 : VTP

Table 2: Stiffness properties of model T-tail.

Case No.	M_∞	V (m/s)	ρ (kg/m^3)	q (kPa)	μ_F	Response	f (Hz)	| H | (mm)
1	0.60	179.7	0.991	16.0	40.3	No flutter		
2			1.114	18.0	35.8	LCO	1.86	64.0
3	0.70	209.7	0.546	12.0	73.1	No flutter		
4			0.637	14.0	62.7	LCO	2.21	82.0
5	0.75	224.7	0.634	16.0	63.0	No flutter		
6			0.714	18.0	56.0	LCO	2.33	110.0
7	0.80	239.6	0.557	16.0	71.7	No flutter		
8			0.626	18.0	63.7	LCO	2.38	109.0
9	0.85	254.6	0.123	4.0	323.5	LCO	5.14*	18.0
10			0.185	6.0	215.7	LCO	4.97*	17.0
11			0.247	8.0	161.8	Flutter	2.91	
12			0.309	10.0	129.4	Flutter	2.88	
13			0.432	14.0	92.4	Flutter	2.55	
14	0.90	269.6	0.165	6.0	241.9	No flutter		
15			0.220	8.0	181.4	Flutter	2.84	
16	0.95	284.6	0.148	6.0	269.5	No flutter		
17			0.296	12.0	134.7	No flutter		
18			0.413	16.7	96.6	No flutter		

* Second mode predominant

Table 3: Results of aeroelastic response computations for α_H= 0 deg.

Case No.	M_∞	V (m/s)	ρ (kg/m^3)	q (kPa)	μ_F	Response	f (Hz)	| H | (mm)
1	0.60	179.7	1.239	20.0	32.2	No flutter		
2	0.70	209.7	0.910	20.0	43.9	No flutter		
3	0.75	224.7	0.554	14.0	72.0	No flutter		
4			0.634	16.0	63.0	Flutter	2.60	
5			0.713	18.0	56.0	Flutter	2.58	
6	0.80	239.6	0.697	20.0	57.3	No flutter		
7	0.85	254.6	0.123	4.0	323.5	No flutter		
8			0.185	6.0	215.7	LCO	2.75	52.0
9			0.247	8.0	161.8	LCO	2.76	39.0
10			0.339	11.0	117.6	LCO	2.80	61.0
11			0.413	13.4	96.6	LCO	2.52	90.0
12	0.90	269.6	0.110	4.0	362.8	LCO	3.09	36.0
13			0.165	6.0	241.9	LCO	2.99	25.0
14			0.220	8.0	181.4	LCO	2.91	23.0
15			0.275	10.0	145.1	LCO	2.88	34.0
16			0.413	15.0	96.7	LCO	2.64	59.0
17	0.95	284.6	0.0988	4.0	404.3	Flutter	3.12	
18			0.148	6.0	269.5	Flutter	3.08	
19			0.198	8.0	202.1	LCO	3.11	12.0
20			0.247	10.0	161.7	LCO	3.13	14.0
21			0.412	16.7	96.8	LCO	3.21	12.0
22	1.00	299.5	0.178	8.0	223.9	No flutter		
23			0.415	18.6	96.3	No flutter		

Table 4: Results of aeroelastic response computations for α_H= 5 deg.